

Deep Generalized Schrödinger Bridges: From Image Generation to Solving Mean-Field Games

Guan-Horng Liu^{*,†}

Fundamental AI Research (FAIR), Meta

GHLIU@META.COM

Tianrong Chen[†]

Apple Machine Learning Research

TCHEN54@APPLE.COM

Evangelos A. Theodorou

Georgia Institute of Technology

EVANGELOS.THEODOROU@GATECH.EDU

Abstract

Generalized Schrödinger Bridges (GSBs) are a fundamental mathematical framework used to analyze the most likely particle evolution based on the principle of least action including kinetic and potential energy. In parallel to their well-established presence in the theoretical realms of quantum mechanics and optimal transport, this paper focuses on an algorithmic perspective, aiming to enhance practical usage. Our motivated observation is that transportation problems with the optimality structures delineated by GSBs are pervasive across various scientific domains, such as generative modeling in machine learning, mean-field games in stochastic control, and more. Exploring the intrinsic connection between the mathematical modeling of GSBs and the modern algorithmic characterization therefore presents a crucial, yet untapped, avenue. In this paper, we reinterpret GSBs as probabilistic models and demonstrate that, with a delicate mathematical tool known as the nonlinear Feynman-Kac lemma, rich algorithmic concepts, such as likelihoods, variational gaps, and temporal differences, emerge naturally from the optimality structures of GSBs. The resulting computational framework, driven by deep learning and neural networks, operates in a fully continuous state space (*i.e.*, mesh-free) and satisfies distribution constraints, setting it apart from prior numerical solvers relying on spatial discretization or constraint relaxation. We demonstrate the efficacy of our method in generative modeling and mean-field games, highlighting its transformative applications at the intersection of mathematical modeling, stochastic process, control, and machine learning.

Keywords: Generalized Schrödinger Bridge, deep learning, stochastic control, nonlinear Feynman-Kac lemma, generative modeling, mean-field games

1 Introduction

The Schrödinger Bridge (SB) problems (Schrödinger, 1931, 1932), originally proposed by Erwin Schrödinger in the 1930s, ask the following question: What is the most likely probability distribution for i.i.d. Brownian particles at an intermediate time given their distributions observed at two distinct time instants? Initially introduced to interpret quantum mechanics (Fortet, 1940), the problem has expanded in scope and gained broader relevance in connection to stochastic control (Pavon and Wakolbinger, 1991; Dai Pra, 1991) and optimal transport (Léonard, 2012; Chen et al., 2021). Nowadays, SBs are well characterized as entropy-regularized optimal transport problems (Peyré and Cuturi, 2017; Léonard, 2013), seeking optimal stochastic processes between two distributions that minimize kinetic energy.

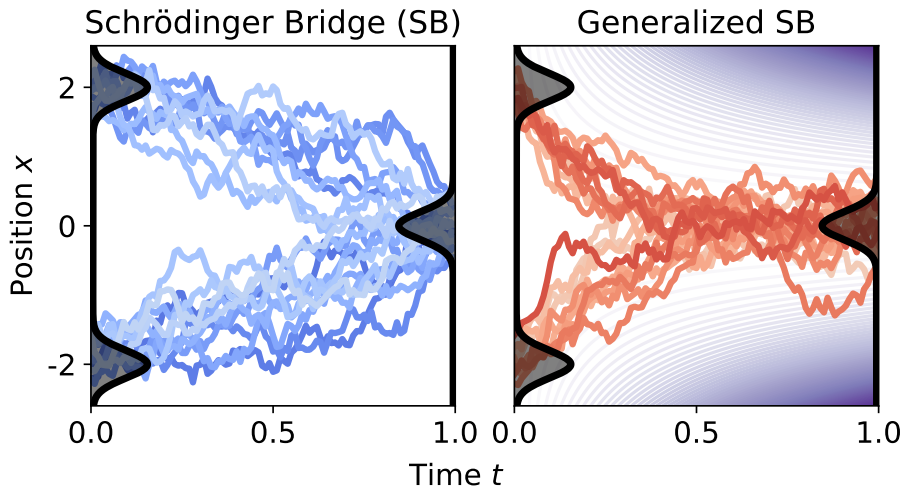


Figure 1: Illustration of **Schrödinger Bridge (SB)** and **Generalized SB** on a 1-dimensional example w.r.t. a time-varying potential energy (purple contours). While SB seeks stochastic processes with minimal kinetic energy, GSB instead considers processes that jointly minimize both kinetic and potential energies.

Mathematically, given a pair of boundary distributions $\mu(\cdot), \nu(\cdot) \in \mathcal{P}(\mathbb{R}^d)$, where $\mathcal{P}(\mathbb{R}^d)$ is the space of probability distributions, SB seeks a pair of differential stochastic processes (SDEs) transporting particles between $\mu(\cdot)$ and $\nu(\cdot)$

$$dX_t = \sigma^2 \nabla \log \Psi(X_t, t) dt + \sigma dW_t, \quad X_0 \sim \mu, \quad X_1 \sim \nu, \quad (1a)$$

$$d\bar{X}_s = \sigma^2 \nabla \log \hat{\Psi}(\bar{X}_s, s) ds + \sigma dW_s, \quad \bar{X}_0 \sim \nu, \quad \bar{X}_1 \sim \mu, \quad (1b)$$

where $W_t \in \mathbb{R}^d$ is the Wiener process, $\sigma \in \mathbb{R}$ is some diffusion scalar known in prior, and ∇ is the gradient operator taken w.r.t. the spatial variable $X_t \in \mathbb{R}^d$. One can understand X_t as a standard stochastic process evolving *forwardly* along the time coordinate $t \in [0, 1]$, whereas \bar{X}_s evolves along the *backward* time coordinate $s := 1 - t$. These two SDEs are the “reversed” process to each other—in the sense that the path measure induced by Equation 1a is equal almost surely to the one induced by Equation 1b. Furthermore, the functions $\Psi, \hat{\Psi} \in C^{2,1}(\mathbb{R}^d, [0, 1])$ obey the following optimality conditions characterized by two partial differential equations (PDEs)

$$\begin{aligned} \partial_t \Psi(x, t) &= -\frac{1}{2} \sigma^2 \Delta \Psi(x, t), & \partial_t \hat{\Psi}(x, t) &= \frac{1}{2} \sigma^2 \Delta \hat{\Psi}(x, t) \\ \text{s.t. } \Psi(x, 0) \hat{\Psi}(x, 0) &= \mu(x), & \Psi(x, 1) \hat{\Psi}(x, 1) &= \nu(x), \end{aligned}$$

where Δ is the Laplacian operator taken w.r.t. the spatial variable.

Despite that stochastic processes with minimal kinetic energy has proven versatile, finding popularity in signal processing (Santambrogio, 2015; Kolouri et al., 2017), computer graphics (Solomon et al., 2015; Solomon, 2018), and statistical inference (Cuturi and Doucet,

2014; Srivastava et al., 2018), it corresponds to the squared-Euclidean transport cost among a range of available alternatives (Di Marino et al., 2017; Koshizuka and Sato, 2023; Cuturi et al., 2023). A crucial extension, as focused in this paper, is the Generalized Schrödinger Bridge (GSB), which introduces an additional layer of complexity by incorporating potential energy into the principle of least action. This departure from traditional SB models allows for application-specific adaptability, unlocking prevalent problems in general scientific domains where the influence of potential energy is significant, including economics (Achdou et al., 2014, 2022), opinion modeling (Schweighofer et al., 2020; Gaitonde et al., 2021), population modeling (Liu et al., 2018; Achdou et al., 2020), computational chemistry and biology (Philippidis et al., 1979; Bunne et al., 2023).

The solutions to GSBs obey the same stochastic dynamics as in Equation 1, except that $\Psi, \widehat{\Psi}$ now solve the following PDEs

$$\begin{aligned} \partial_t \Psi(x, t) &= V(x, t)\Psi(x, t) - \frac{1}{2}\sigma^2 \Delta \Psi(x, t), & \partial_t \widehat{\Psi}(x, t) &= -V(x, t)\widehat{\Psi}(x, t) + \frac{1}{2}\sigma^2 \Delta \widehat{\Psi}(x, t) \\ \text{s.t. } \Psi(x, 0)\widehat{\Psi}(x, 0) &= \mu(x), & \Psi(x, 1)\widehat{\Psi}(x, 1) &= \nu(x), \end{aligned} \quad (2)$$

where $V(x, t) : \mathbb{R}^d \times [0, 1] \rightarrow \mathbb{R}$ is the *potential energy*. When $V := 0$ vanishes, Equation 2 reduces to standard SB problems. In other words, GSBs *generalizes* SBs with nontrivial potential energy $V(x, t)$.

Due to the coupling at the boundary conditions w.r.t. μ and ν , the PDEs in Equation 2 lack analytic solutions, even in the absence of $V(x, t)$. Consequently, conventional numerical methods for solving GSBs (and SBs) typically sidestep direct PDE solutions, opting instead for algorithms such as the Sinkhorn methods (Sinkhorn and Knopp, 1967; Knight, 2008; Cuturi, 2013), which, despite their superior convergence and stability, require mesh-based discretization (Caluya and Halder, 2021; Chen, 2023) of the state space. Even with the aid of deep learning, modern deep PDE solvers struggle to handle the boundary constraints, often necessitating the relaxation of these distributional constraints as soft penalties (Ruthotto et al., 2020; Lin et al., 2021). Given that problems involving the transportation of samples between two distributions are prevalent across scientific applications, with generative modeling (Song et al., 2021; Lipman et al., 2023) being notable examples,¹ the introduction of modern algorithmic concepts in solving GSBs, or how GSBs shall be interpreted from a practical machine learner perspective, remains a crucial yet unexplored avenue.

In this paper, we elucidate the intricate process of deconstructing GSBs into fundamental components, leveraging a delicate mathematical tool known as the nonlinear Feynman-Kac lemma in stochastic process and control (Ma et al., 1999; Han et al., 2018; Exarchos and Theodorou, 2018). From which, we construct a deep learning-based computational framework capable of solving GSBs. Specifically, we interpret GSBs as probabilistic models by casting them as Neural SDEs (Li et al., 2020; Kidger et al., 2021), a family of parametric SDEs wherein drifts (and sometimes diffusions) are parametrized by deep neural networks. We demonstrate that maximizing their likelihoods effectively enforces the distributional boundary constraints in Equation 1. Simultaneously, temporal differences, originally appearing in reinforcement learning (Wiering and Van Otterlo, 2012; Szepesvári, 2022), play a crucial role in ensuring that particle trajectories adhere to the principle of least action,

1. In this context, μ and ν refer to Gaussian prior and empirical data distribution.

encompassing both kinetic and, if present, potential energy. The emergence of these common learning objectives from the PDEs in Equation 2 strengthens the intrinsic connection between mathematical modeling, stochastic control, and machine learning.

Built upon these novel learning objectives, we present two practical algorithms, one applicable to solving GSB problems while another specialized for solving SBs, *i.e.*, when the primary focus is on determining transportation with minimal kinetic energy. Given that the latter learning scheme are relatively well-studied, owing to recent advances in training SBs (De Bortoli et al., 2021; Vargas et al., 2021) despite arising from different perspectives, we provide new theoretical results for the first, more general learning algorithm for GSBs. Specifically, we prove that jointly optimizing the combined objectives of likelihoods and temporal differences is sufficient for the parametrized Neural SDEs to recover the solutions to GSB. Highlighting the efficacy and broad applicability of these two learning algorithms, we demonstrate their performance in image generation and solving mean-field games, where the potential energy plays a crucial role in quantifying physical constraints and interactions within individual and large populations.

2 Methodology

In this section, we present our deep learning-based computational framework for solving GSBs (and SBs). The proofs of all theorems can be found in Appendix A.

2.1 GSBs as Probabilistic Models

The solutions to the SDEs in Equation 1 define forward and backward transport maps between the distributions μ and ν . Since the transport maps are, by construction, stochastic, they can be interpreted as probabilistic models—in the sense that one can *generate* samples from, *e.g.*, $\nu(\cdot)$ by solving Equation 1a, and vice versa. In this vein, we consider the following representations of GSBs, instantiating a recent class of neural differential equations (Chen et al., 2018) known as Neural SDEs (Li et al., 2020)

$$dX_t^\theta = \sigma Z^\theta(X_t^\theta, t)dt + \sigma dW_t, \quad X_0 \sim \mu, \quad (3)$$

$$d\bar{X}_s^\phi = \sigma \hat{Z}^\phi(\bar{X}_s^\phi, s)ds + \sigma dW_s, \quad \bar{X}_0 \sim \nu, \quad (4)$$

where $Z^\theta \approx \sigma \nabla \log \Psi$ and $\hat{Z}^\phi \approx \sigma \nabla \log \hat{\Psi}$ are learnable functions, aiming to approximate the drifts in Equation 1, with θ and ϕ gathering their learnable parameters. The superscripts in X_t^θ and \bar{X}_s^ϕ highlight their dependency on the parameters θ and ϕ .

2.2 Stochastic Representation of Equation 2

Given trajectories simulated from Equation 3, or Equation 4, we wish to design learning objectives that enforce the optimality conditions in Equation 2. Unfortunately, the PDEs in Equation 2 are not immediately applicable, as they describe the spatial-temporal relation in a point-wise fashion across the product space of $\mathbb{R}^d \times [0, 1]$, as opposed to how the functions shall be evaluated along stochastic processes, which are nowhere differentiable. This necessitates a *stochastic* representation of Equation 2 in which (x, t) evolves according to some stochastic process, as shown in the following Theorem 1.

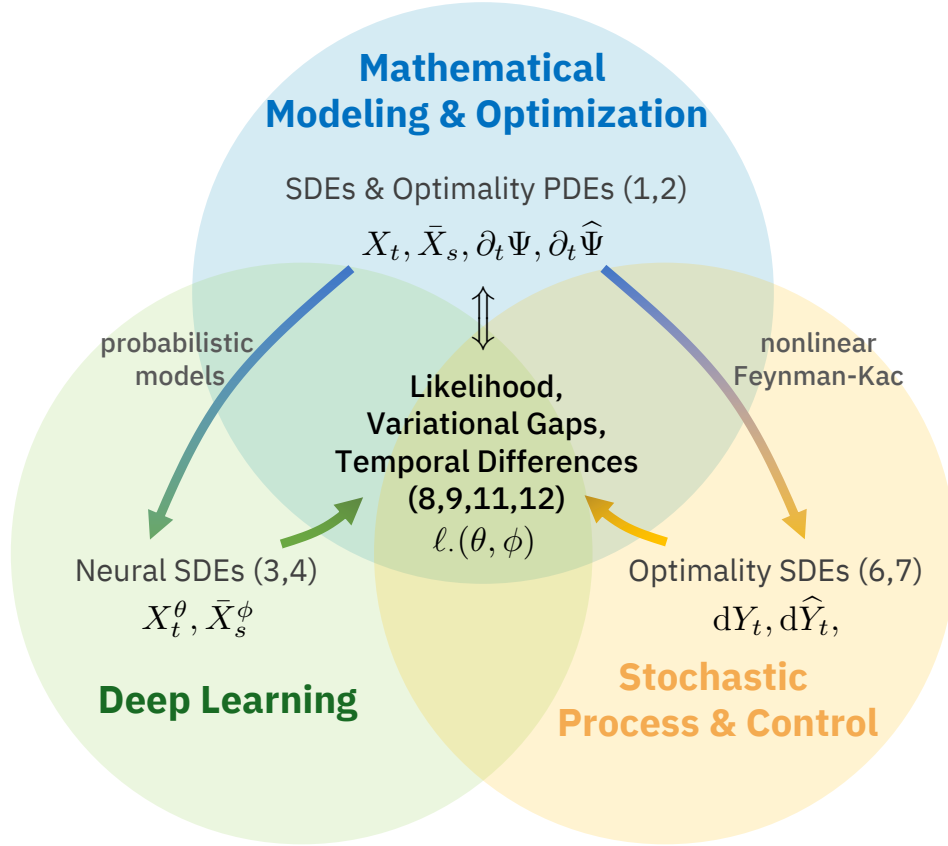


Figure 2: Overview of our methodology. We begin with the mathematical foundation of Generalized Schrödinger Bridges (GSBs) and SBs, which are characterized by the SDEs in Equation 1 and their optimality conditions represented as PDEs in Equation 2. We propose a novel perspective, casting these SDEs as probabilistic models that construct stochastic transport maps between samples drawn from two different distributions, leading to a parametrization with Neural SDEs. On the other hand, the optimality PDEs conditions in Equation 2 admit stochastic representation and can be transformed into computationally more tractable *optimality SDEs* in Equations 6 and 7 via a mathematical tool known as the nonlinear Feynman-Kac lemma (*i.e.*, Theorem 1). This transformation facilitates the emergence of common learning objectives such as likelihoods in Equations 8 and 9, variational gaps (Theorem 2), and temporal differences in Equations 11 and 12. We show in Theorem 3 that optimizing the combined objectives provides necessary and sufficient conditions to GSB solutions, making them apt for learning approximate solutions of GSBs. In essence, our work reveals an intrinsic connection between mathematical modeling of GSBs, stochastic processes, control, and deep learning.

Theorem 1 Consider the random variables

$$Y_t := \log \Psi(X_t, t), \quad \widehat{Y}_t := \log \widehat{\Psi}(X_t, t), \quad (5)$$

where X_t solves Equation 1a. Then, Y_t and \widehat{Y}_t solve

$$dY_t = \left(\frac{1}{2} \|\sigma \nabla Y_t\|^2 + V \right) dt + \sigma \nabla Y_t \cdot dW_t, \quad (6)$$

$$d\widehat{Y}_t = \left(\frac{1}{2} \|\sigma \nabla \widehat{Y}_t\|^2 - V + \nabla \cdot (\sigma^2 \nabla \widehat{Y}_t) + \sigma^2 \nabla \widehat{Y}_t \cdot \nabla Y_t \right) dt + \sigma \nabla \widehat{Y}_t \cdot dW_t. \quad (7)$$

The solutions to the PDEs in Equation 2 can be recovered via taking conditional expectation:

$$\mathbb{E}[Y_t | X_t = x] = \log \Psi(x, t), \quad \mathbb{E}[\widehat{Y}_t | X_t = x] = \log \widehat{\Psi}(x, t).$$

Theorem 1 stems directly from the nonlinear Feynman-Kac lemma (Ma et al., 1999; Han et al., 2018), providing a stochastic representation (in terms of Y_t and \widehat{Y}_t) of the optimality PDE conditions in Equation 2 by characterizing how their function values change along the SDE X_t in Equation 1a. Notably, their values evolve as another set of SDEs. Such transformations, bridging specific classes of PDEs and SDEs, have become prominent in recent advancements in numerical methods for stochastic control (Exarchos and Theodorou, 2018; Pereira et al., 2019a). Importantly, rather than solving the PDEs in the entire function space, it suffices to solve them locally around high probability regions induced by the SDE. We will solidify the connection to stochastic control shortly.

2.3 Likelihood Objective

With Theorem 1, we can now derive the model likelihood (Myung, 2003), a prevalent objective in learning probabilistic models. The standard procedure is to minimize the negative log-likelihood, which, in our case, would be computed from the Neural SDEs. Consider the *forward* Neural SDE in Equation 3, for instance. Given a trajectory simulated from $X_0 \sim \mu$, our goal is to estimate

$$\log \mu^\theta(X_0) \approx \log \Psi(X_0, 0) + \log \widehat{\Psi}(X_0, 0),$$

where the approximation follows from the boundary condition in Equation 2. In other words, we wish to estimate $\log \Psi$ and $\log \widehat{\Psi}$ given $X_{t \in [0,1]}^\theta$. Applying Theorem 1 suggests the objective

$$\ell_{\text{fwd}}(\theta, \phi) = -\mathbb{E} \left[Y_0 + \widehat{Y}_0 | X_0 \right] = \int_0^1 \mathbb{E} \left[\frac{1}{2} \|Z_t^\theta + \widehat{Z}_t^\phi\|^2 + \nabla \cdot (\sigma \widehat{Z}_t^\phi) \right] dt - \mathbb{E} \log \nu(X_1^\theta), \quad (8)$$

where we substitute $\sigma \nabla Y_t \approx Z_t^\theta(X_t^\theta, t)$, $\sigma \nabla \widehat{Y}_t \approx \widehat{Z}_t^\phi(X_t^\theta, t)$ and shorthand them respectively by Z_t^θ and \widehat{Z}_t^ϕ . Notice that the Itô integrals vanish due to the martingale property.

Repeating similar derivation for the backward Neural SDE in Equation 4, except now along the reversed time coordinate s , yields the likelihood objective for $\log \nu^\phi(\bar{X}_0)$

$$\ell_{\text{bwd}}(\phi, \theta) = \int_0^1 \mathbb{E} \left[\frac{1}{2} \|Z_s^\theta + \widehat{Z}_s^\phi\|^2 + \nabla \cdot (\sigma Z_s^\theta) \right] ds - \mathbb{E} \log \mu(\bar{X}_1^\phi), \quad (9)$$

where we substitute $\sigma \nabla Y_s \approx Z_s^\theta(\bar{X}_s^\phi, s) \equiv Z_s^\theta$ and $\sigma \nabla \widehat{Y}_s \approx \widehat{Z}_s^\phi(\bar{X}_s^\phi, s) \equiv \widehat{Z}_s^\phi$, similar to Equation 8.

2.4 Variational Gap of ℓ_{fwd} and ℓ_{bwd}

It should be noted that Theorem 1 provides characterization only at the equilibrium, *i.e.*, when X_t 's follow the *optimal* solutions in Equation 1a. Due to the parametrization, Equations 8 and 9 present the variational bounds. This raises questions of whether minimizing Equations 8 and 9 suffices to close the variational gaps. We provide a positive answer in the following result.

Theorem 2 *Let p^θ and p^ϕ denote the path densities induced respectively by the Neural SDEs in Equations 3 and 4. Then,*

$$\ell_{\text{fwd}}(\theta, \phi) = D_{\text{KL}}(p^\theta || p^\phi) - \log \mu^\theta(X_0), \quad \ell_{\text{bwd}}(\phi, \theta) = D_{\text{KL}}(p^\phi || p^\theta) - \log \nu^\phi(\bar{X}_0),$$

where $D_{\text{KL}}(\cdot || \cdot)$ is the Kullback-Leibler (KL) divergence, and μ^θ and ν^ϕ are the parametrized model likelihoods. Furthermore, their optimal values achieve the true likelihoods, *i.e.*,

$$-\log \mu(X_0) = \min_{\theta, \phi} \ell_{\text{fwd}}(\theta, \phi), \quad -\log \nu(\bar{X}_0) = \min_{\phi, \theta} \ell_{\text{bwd}}(\phi, \theta).$$

Theorem 2 suggests that the variational gaps can be quantified by the KL divergences between two Neural SDEs. Take $\ell_{\text{fwd}}(\theta, \phi)$ for instance. Since ϕ appears only in the KL divergence, the minimizer ϕ must obey $p^{\phi^*} = p^\theta$ for $t \in [0, 1)$. Minimizing $\ell_{\text{fwd}}(\theta, \phi)$ w.r.t. θ thereby amounts to maximum likelihood estimation, justifying the use of Equations 8 and 9 in practice. Essentially, the likelihood objectives $\ell_{\text{fwd}}(\theta, \phi)$ and $\ell_{\text{bwd}}(\phi, \theta)$ ensure the terminal distributions of the Neural SDEs in Equations 3 and 4 to satisfy the distributional constraints. This, crucially, distinguishes our proposed framework from prior attempts built also upon neural differential equations (Ruthotto et al., 2020; Lin et al., 2021), which require *relaxing* the distributional constraint with soft penalty. We highlight this distinction arising from the delicate transformation of the PDE constraints in Equation 2 to the SDEs in Equations 6 and 7.

Despite being encouraging, the results in Theorem 2 is *insufficient* in showing the minimizers of ℓ_{fwd} , or ℓ_{bwd} , solve GSBs. This is best explained by revisiting Equations 6 and 7, and notice that the two terms related to potential energy, $+V$ and $-V$, cancel out in the computation of the likelihood objective in Equation 8. In other words, the likelihood objectives remain the same regardless of the choices of $V(x, t)$, ensuring the distributional boundary constraints yet not necessarily the optimality of the trajectories in between. Below, we discuss a simple remedy inspired by stochastic control, further strengthening the interconnection of our proposed framework across diverse research fields.

2.5 Temporal Difference (TD) Objective

Let us revisit the random variable Y_t and its connection to the PDEs in Equation 2. These PDEs admit an intriguing variational formulation, in that they are the optimality conditions to following constrained optimization

$$\min_u \int_0^1 \mathbb{E} \left[\frac{1}{2} \|u(X_t, t)\|^2 + V(X_t, t) \right] dt, \quad \text{s.t. } dX_t = \sigma u(X_t, t)dt + \sigma dW_t, \quad X_0 \sim \mu, \quad X_1 \sim \nu. \quad (10)$$

The variational formulation provides an intuitive interpretation to the potential energy $V(x, t)$. Essentially, GSB solves a stochastic optimal control (SOC) with distributional boundary constraints, where, among all the controlled processes that transport samples from $\mu(\cdot)$ to $\nu(\cdot)$, it considers the one with the least kinetic, presenting as the velocity norm, and potential energy to be optimal.

Serving as the optimality conditions to the constrained SOC in Equation 10, the PDEs in Equation 2 share the same roles as the Hamilton-Jacobi-Bellman (HJB) equation appearing in SOC literature (Kappen, 2005; Exarchos and Theodorou, 2018), with $\log \Psi(x, t)$ resembling the value function.² In other words, the random variable $Y_t := \log \Psi(X_t, t)$ can be understood as the unique stochastic representation of the value function evaluated along the process X_t . This implies that the dynamics of Y_t evolve according to the Bellman equation (Bellman, 1954), except in a stochastic, continuous-time fashion. Indeed, discretizing Equation 6 with some fixed step size δt and $\delta W_t \sim \mathcal{N}(0, \delta t)$ yields

$$Y_{t+\delta t} = Y_t + \left(\frac{1}{2} \|\sigma \nabla Y_t\|^2 + V \right) \delta t + \sigma \nabla Y_t \cdot \delta W_t,$$

which resembles a non-discounted temporal difference (Todorov, 2009; Lutter et al., 2021), with the distinction that, beyond the usual “rewards” associated with control and state costs, a stochastic term is introduced. Unlike the conventional Bellman equation where this stochastic term disappears upon expectation, here it plays a critical role in characterizing the intrinsic stochasticity of Y_t and exhibits further connections to the optimal control variate (Robert et al., 1999; Richter and Berner, 2022).

With the interpretation in mind, we consider $Y^\theta \approx \log \Psi$ and $\hat{Y}^\phi \approx \log \hat{\Psi}$ and re-parametrize the drifts of Neural SDEs by $Z_t^\theta := \sigma \nabla Y^\theta$ and $\hat{Z}_t^\phi := \sigma \nabla \hat{Y}^\phi$. Then, the TD objectives can be constructed as follows

$$\ell_{\text{TD}}(\theta) = \mathbb{E} \left\| Y_{t+\delta t}^\theta - \left(Y_t^\theta + \left(\frac{1}{2} \|Z_t^\theta\|^2 + V \right) \delta t + Z_t^\theta \cdot \delta W_t \right) \right\|^2, \quad (11)$$

$$\ell_{\text{TD}}(\phi) = \mathbb{E} \left\| \hat{Y}_{t+\delta t}^\phi - \left(\hat{Y}_t^\phi + \left(\frac{1}{2} \|\hat{Z}_t^\phi\|^2 - V + \nabla \cdot (\sigma \hat{Z}_t^\phi) + \hat{Z}_t^\phi \cdot Z_t^\theta \right) \delta t + \hat{Z}_t^\phi \cdot \delta W_t \right) \right\|^2, \quad (12)$$

where $\check{\theta}$ and $\check{\phi}$ denote the detached copy of the parameters. The expectations in Equations 11 and 12 are taken w.r.t. the stochasticity induced in the Neural SDE in Equation 3, with t sampled uniformly between $[0, 1]$. Our final result suggests that adding these TD objectives to the likelihood objective suffices to recover GSBs.

Theorem 3 $Y^\theta, \hat{Y}^\phi, Z^\theta,$ and \hat{Z}^ϕ solve the GSB problem if and only if they are the minimizers of $\ell_{\text{fwd}}(\theta, \phi) + \ell_{\text{TD}}(\phi)$

Theorem 3 can be easily extended to different combinations with $\ell_{\text{bwd}}(\phi, \theta)$ and $\ell_{\text{TD}}(\theta)$.

2.6 Joint and Alternate Training Schemes

Theorem 3 validates a training scheme where we jointly learn the parameters θ, ϕ

$$\min_{\theta, \phi} \ell_{\text{fwd}}(\theta, \phi) + \ell_{\text{TD}}(\phi). \quad (13)$$

2. These interpretations can be made concrete; see Appendix B.1 for more detailed discussions.

Though joint training works well in low-to-moderate dimensional problems, it necessitates back-propagating through the Neural SDE (notice, for instance, that computing $\ell_{\text{fwd}}(\theta, \phi)$ requires simulating $X_{t \in [0,1]}^\theta$), which becomes prohibitively expensive as the dimension d grows. An alternative is to alternate between minimizing $\ell_{\text{fwd}}(\theta, \phi)$ and $\ell_{\text{fwd}}(\phi, \theta)$ but only w.r.t. the second input:

$$\phi^{(k)} \leftarrow \arg \min_{\phi} \ell_{\text{fwd}}(\theta^{(k)}, \phi), \quad \theta^{(k+1)} \leftarrow \arg \min_{\theta} \ell_{\text{bwd}}(\phi^{(k)}, \theta). \quad (14)$$

From Theorem 2, Equation 14 is equivalent to alternate minimization of the KL divergences, as the likelihoods are now independent of the optimized variables and hence can be dropped. This alternate procedure instantiates the Iterative Proportional Fitting algorithm (Kullback, 1968), commonly adopted for solving SBs (Vargas et al., 2021). Despite being applicable only when $V := 0$, it stands as a pragmatic adjustment when least kinetic energy alone suits the applications, as demonstrated in the subsequent section.

3 Numerical Experiments

In this section, we validate our proposed deep learning-based framework, *i.e.*, Equations 13 and 14, in solving SBs and GSBs. We focus on two distinct applications—generative modeling and solving mean-field games—aiming to highlight the extensive applicability of SBs and GSBs in diverse scientific areas.

3.1 Generative Modeling with Alternate Training

Generative modeling stands at the forefront of modern machine learning, playing a pivotal role in transforming various industries and everyday experiences with cutting-edge tools like GPT-4 (Achiam et al., 2023) and Stable Diffusion (Rombach et al., 2022). At its core, generative models aim to discern the underlying data distribution given only empirical samples. Once learned, the models can be used to sample or, equivalently, *generate* new data and content. Advanced deep generative models, exemplified by flow or diffusion models (Lipman et al., 2023; Song et al., 2021), strive to identify neural differential equations capable of mapping simple distributions, typically Gaussian, into complex, often intractable, data distributions. Adopting our notations, let

$$\mu(x) := \mathcal{N}(x), \quad \nu(x) := p_{\text{data}}(x),$$

where \mathcal{N} and p_{data} denotes respectively normal and data distributions. Then, SBs solve a set of Neural SDEs transporting samples back-and-forth between the two distributions with minimal kinetic energy. Notably, the kinetic regularization has been shown effectively in enhancing training and sampling efficiency (Finlay et al., 2020; Chen et al., 2022; Shaul et al., 2023).

Regarding the choice of p_{data} , we explore three data sets, namely MNIST (LeCun et al., 2010), CelebA (Liu et al., 2015), and Cifar10 (Krizhevsky, 2009), each representing different image domains. MNIST consists of 60,000 handwritten digits, CelebA features 202,599 images of celebrities’ faces, and Cifar10 contains 60,000 objects categorized into ten classes, such as airplanes, cars, birds, cats, deer, dogs, frogs, horses, ships, and trucks. These data

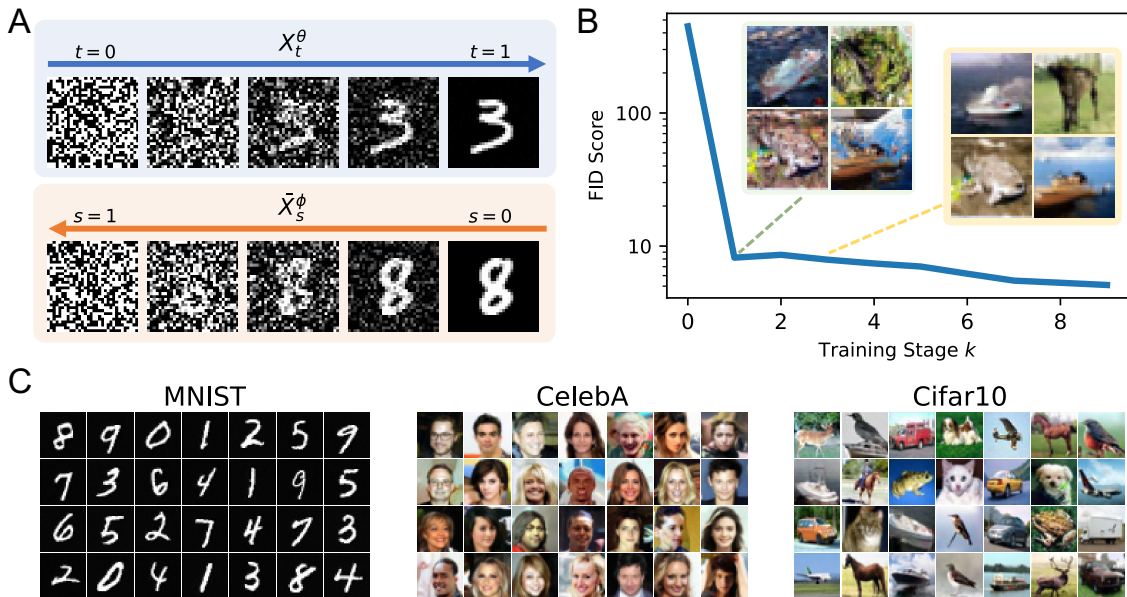


Figure 3: Results of generative modeling in image domains. (A) Simulations of the learned Neural SDEs, exemplified with a handwritten digit data set MNIST. While X_t^θ evolves along the forward time coordinate t , transforming a Gaussian noise to an image (in this case a digit 3), \bar{X}_s^ϕ instead moves backward along the coordinate $s := 1 - t$ and generates random noises. (B) Training progress of Cifar10 with respect to the Fréchet Inception Distance (FID) score. Notice how the the FID score stably decreases, improving the fidelity of the generated images over time. (C) Generated samples, *i.e.*, X_1^θ , on all three tested data sets, including MNIST (left), CelebA (middle), and Cifar10 (right).

sets are selected not only for their popularity in the machine learning community but to diversify the distribution being modeled. MNIST represents discrete data in gray scale, while both CelebA and Cifar10 consist of color images. Additionally, Cifar10 encompasses a variety of natural images across different categories, whereas CelebA focuses on facial attributes. All images are resized to 32 by 32 resolution, resulting in problem dimensions of $d = 1024$ for MNIST and $d = 3072$ for CelebA and Cifar10. We employ the alternate training scheme in Equation 14 to train an SB on each data set.

The learning results are summarized in Fig. 3, demonstrating the effectiveness of the proposed computational framework as a generative model in synthesizing high-fidelity images, by learning transport maps between Gaussian priors and image distributions. Notably, in Fig. 3A, the forward Neural SDE X_t^θ learns to generate images from random noises, while the backward Neural SDE \bar{X}_s^ϕ reverses the generative process. This training of SBs is therefore reminiscent of diffusion models, as pointed out in De Bortoli et al. (2021); Vargas et al. (2021); Chen et al. (2022), except that the stochastic processes from data to noises are learned rather than prescribed. Quantitatively, Fig. 3B tracks the performance of modeling

Cifar10 during training, measured by the Fréchet Inception Distance (FID) score (Heusel et al., 2017), a commonly-used metrics for evaluating the proximity of the generated distribution to the empirical data distribution. The decreasing FID score throughout training indicates an enhancement in the quality of generated images. This improvement is further confirmed by examining images generated at different training stages while freezing the random seeds and initial states, revealing a distinguishable reduction in visible flaws.

3.2 Mean-Field Games (MFGs) with Joint Training

MFGs constitute a crucial mathematical framework in modeling the collective behavior of individual agents interacting stochastically with a large population. This framework is prevalent across multidisciplinary scientific areas (Achdou et al., 2014, 2022; Schweighofer et al., 2020; Gaitonde et al., 2021; Liu et al., 2018; Achdou et al., 2020), delineating a non-cooperative differential game involving *a continuum population of rational agents*. Here, “continuum” refers to the scenario where the number of agents in a multi-agent game approaches infinity (hence the term *mean-field*), resulting in the interaction between individuals and population density. On the other hand, “rationality” relies on some variational structure to which the collective behavior of individuals must adhere.

We focus on classical examples of crowd navigation in \mathbb{R}^2 . Our goal is to understand how rational agents navigate between the population distributions observed at two distinct snapshots. Rationality, in this context, involves several objectives:

1. Minimizing execution efforts from one point to another.
2. Considering interactions between individuals and population, such as avoiding crowded or congested regions with high probability density.
3. Avoiding physical constraints, such as obstacles.

To explore how GSBs can be applied to solve MFGs, we observe that the first objective aligns with the kinetic energy, representing the total control spent in transporting samples between two distributions. Meanwhile, the second and third objectives influence agents’ behaviors by imposing preferences through their “state” rather than the executed control, making them applicable as the potential energy $V(x, t)$. Indeed, crowd navigation MFGs are conventionally framed as the distribution-constrained SOC (Ruthotto et al., 2020; Lin et al., 2021), where $V(x, t)$ either measures the cost incurred for individuals to stay in densely crowded regions with high population density such as entropy or congestion cost (Ruthotto et al., 2020; Lin et al., 2021) or restricted area such as obstacles

$$V_{\text{ent}}(x, t) := \log \rho(x, t), \quad V_{\text{cgst}}(x, t) := \mathbb{E}_{y \sim \rho} \left[\frac{1}{\|x - y\|^2 + 1} \right], \quad V_{\text{obs}}(x, t) := c \cdot \mathbb{1}_{\text{obs}}(x),$$

where c is a tuning hyper-parameter and $\mathbb{1}_{\text{obs}}(\cdot)$ denotes the indicator of the problem-dependent obstacle set.

We examine three crowd navigation MFGs from the literature (Ruthotto et al., 2020; Lin et al., 2021; Liu et al., 2022), encompassing (i) asymmetric obstacle avoidance, (ii) entropy interaction with a V-shaped bottleneck, and (iii) congestion interaction on an S-shaped tunnel. Figure 4A depicts the configuration of each MFG, denoted as *GMM*, *V-neck*,

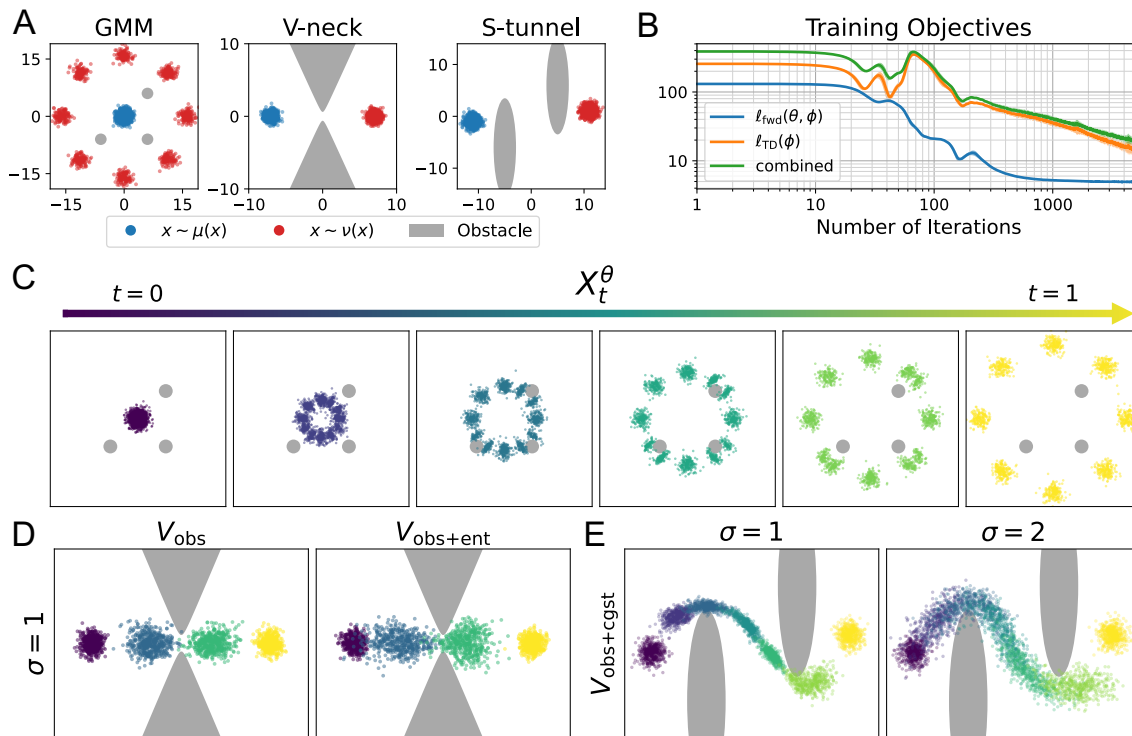


Figure 4: Results of mean-field games (MFGs) in crowd navigation scenarios. (A) The configurations of three distinct MFGs, namely GMM, V-neck, and S-tunnel, showcasing the boundary distributions μ (blue), ν (red), and restricted areas (gray). (B) Training progress of GMM, providing insights into how the likelihood and temporal difference (TD) objectives contribute to the combined training objective. We report the average over 5 random seeds. (C) The simulation results on GMM, where seven population snapshots are displayed at regular intervals between $t \in [0, 1]$, each with a different color. (D and E) Additionally, an ablation study is conducted on the entropy interaction cost and diffusion coefficient σ for V-neck and S-tunnel, respectively. For optimal visualization, four population snapshots are presented for V-neck, and seven for S-tunnel.

and *S-tunnel*, respectively. For simplicity, we consider Gaussians or mixtures of Gaussians for μ, ν , even though our method is applicable to general distributions, as demonstrated in the previous example. On all three MFGs, we train Generalized Schrödinger Bridges with the combined objectives of likelihoods and temporal differences (TDs) in Equation 13. As illustrated in Fig. 4B, the likelihood objectives typically converge faster than the TD objectives, and the overall training saturates within 4,000-5,000 iterations. Empirically, we observe that joint training of θ, ϕ demonstrates faster convergence than its alternate counterpart, albeit with higher memory consumption.

Our primary outcomes are illustrated in Fig. 4C-E. It is evident that, across all three crowd navigation setups, our method effectively guides the population to navigate smoothly

while avoiding restricted areas (marked gray). A notable difference emerges when the interaction entropy cost is introduced, as shown in Fig. 4D, where the population is encouraged to disperse both before and after navigating through the V-shaped bottleneck. Meanwhile, Fig. 4E demonstrates the robustness of our method w.r.t. different diffusion coefficients σ . Importantly, the learned transport maps satisfy the required distributional boundary constraints in all cases. In summary, our computational framework, serving as a numerical solver for MFGs, exhibits robust performance across diverse setups involving various optimality structures, degrees of stochasticity, and problem configurations.

4 Discussion and Outlook

We present a deep learning-based method for solving Generalized Schrödinger Bridges (GSBs), employing a set of Neural SDEs to transport samples between two distributions while adhering to the variational principle of kinetic and potential energy. Our proposed computational framework falls within the realm of numerical solvers for neural differential equations (Chen et al., 2018), playing a crucial role across diverse scientific domains and bridging the gap between mathematicians and machine learning practitioners. Conventional solvers treat deep neural networks merely as function approximations and base their algorithms on standard optimization procedures, such as Lagrangian (Ruthotto et al., 2020) and PDE regression (Raissi et al., 2019). Our work, in its essence, challenges this paradigm by revealing the inherent connection between variational structures in mathematical models and fundamental concepts in machine learning. This necessitates a fundamental understanding between mathematical modeling, optimization, and deep learning, through which we emphasize the significance of the nonlinear Feynman-Kac lemma, a key tool in the analysis of stochastic processes and control. The integration of machine learning components results in a computational framework that transcends the application boundaries to which the developed method can be applied. We demonstrate this advantage through various applications that may seem unrelated at first glance, ranging from generative modeling for image domains to solving crowd navigation mean-field games in computational social science.

It is worth noticing that the TD objectives inherited in the optimality SDEs Equations 6 and 7 narrow the gap between GSBs and Deep Reinforcement Learning (RL). Notably, the variational formulation in Equation 10 resembles a standard RL problem, seeking an optimal policy that minimizes costs (or equivalently, maximize rewards) along trajectories. However, GSBs distinguish themselves from standard RL setups by introducing a distributional boundary constraint instead of a terminal cost, addressed through an augmented learning objective with a likelihood component. The intriguing use of likelihoods to enforce distribution constraints opens the door to potential advancements leveraging algorithmic developments in the RL community. The application of numerical methods designed for distribution-constrained RL or Stochastic Optimal Control holds promise for providing solutions to previously challenging mean-field games and other social science problems under more realistic settings, aligning with scenarios where social scientists observe population snapshots over time and aim to understand behavior in between these observed intervals or future evolution.

Looking ahead, there are several open questions that warrant exploration. From an application standpoint, the extension of the objective in Equation 10 to encompass general Lagrangian functions $\mathcal{L}(x, \dot{x}, t)$ holds potential significance, as it could unlock applications in metric learning, computational chemistry, and biology. These domains often involve intricate geometry structures that go beyond Euclidean spaces. Furthermore, the extension to incorporate other kinds of stochastic processes, such as jump diffusions, could open avenues for applications in areas like operations research, time series analysis, and finance.

Acknowledgments and Disclosure of Funding

We thank Ioannis Exarchos and Oswin So for their generous involvement and helpful supports; Marcus A Pereira and Ethan N Evans for their participation in the early stage of project exploration; and Bogdon Vlahov for sharing the computational resources. This research was supported by the ARO Award #W911NF2010151 and DoD Basic Research Office Award HQ00342110002.

Appendix A. Proofs

A.1 Preliminaries

We first state some useful equalities that will appear in the proceeding proofs.

- For any point $x \in \mathbb{R}^d$ such that $p(x) \neq 0$, it holds that

$$\begin{aligned} \frac{1}{p(x)} \Delta p(x) &= \frac{1}{p(x)} \nabla \cdot \nabla p(x) = \frac{1}{p(x)} \nabla \cdot \left(p(x) \nabla \log p(x) \right) \\ &= \frac{1}{p(x)} \left(\nabla p(x) \cdot \nabla \log p(x) + p(x) \Delta \log p(x) \right) \\ &= \|\nabla \log p(x)\|^2 + \Delta \log p(x) \end{aligned} \quad (15)$$

- Under mild assumptions (Anderson, 1982; Yong and Zhou, 1999) such that all distributions approach zero at a sufficient speed as $\|x\| \rightarrow \infty$, and that all integrands are bounded, we have

$$\mathbb{E}_{x \sim p(x)} [\Delta \log q(x)] = \mathbb{E}_{x \sim p(x)} [\nabla \cdot \nabla \log q(x)] = \mathbb{E}_{x \sim p(x)} [-\nabla \log p(x) \cdot \nabla \log q(x)], \quad (16)$$

where the second equality follows by integration by parts and reparameterization trick

$$\begin{aligned} \int p(x) (\nabla \cdot \nabla \log q(x)) dx &= \int -(\nabla p(x) \cdot \nabla \log q(x)) dx \\ &= \int -p(x) (\nabla \log p(x) \cdot \nabla \log q(x)) dx. \end{aligned}$$

More generally, under the same regularity, it holds for a vector field $Z : \mathbb{R}^d \mapsto \mathbb{R}^d$ that

$$\mathbb{E}_{x \sim p(x)} [\nabla \cdot Z(x)] = \mathbb{E}_{x \sim p(x)} [-\nabla \log p(x) \cdot Z(x)]. \quad (17)$$

- Itô formula (Itô, 1951): Let X_t be the solution to the Itô SDE

$$dX_t = f(X_t, t)dt + \sigma dW_t.$$

Then, the stochastic process $v(X_t, t)$, where $v \in C^{2,1}(\mathbb{R}^d, [0, 1])$, is also an Itô process

$$dv(X_t, t) = \frac{\partial v(X_t, t)}{\partial t} dt + \left[\nabla v(X_t, t) \cdot f + \frac{1}{2} \sigma^2 \Delta v(X_t, t) \right] dt + \sigma \nabla v(X_t, t) \cdot dW_t \quad (18)$$

- Nonlinear Feynman-Kac lemma (): The lemma establishes an innate connection between different classes of PDEs and forward-backward SDEs. Consider the following forward-backward SDEs,

$$\begin{cases} dX_t = f(X_t, t)dt + G(X_t, t)dW_t, & X_0 = x_0 & (19a) \\ dY_t = -h(X_t, Y_t, Z_t, t)dt + Z \cdot dW_t, & Y_1 = \varphi(X_1) & (19b) \end{cases}$$

where the functions f , G , h , and φ satisfy the regularity conditions:

- f , G , h , and φ are continuous,
- f and G are uniformly Lipschitz in x ,
- h satisfies quadratic growth condition in z ,

such that Equation 19 exists a pair of unique strong solutions (Yong and Zhou, 1999; Kobylanski, 2000). Then, the solution to Equation 19 coincides with the solution to the following second-order parabolic PDE $v(x, t) \in C^{2,1}$

$$\partial_t v + \frac{1}{2} \text{Tr}(\nabla^2 v G G^\top) + \nabla v^\top f + h(t, x, v, G^\top \nabla v) = 0, \quad v_1(x) = \varphi(x), \quad (20)$$

in the sense that Y_t equals almost surely to v along the paths generated by Equation 19a, and the following stochastic representation holds

$$v(X_t, t) = Y_t, \quad G(X_t, t)^\top \nabla v(X_t, t) = Z_t. \quad (21)$$

Intuitively, since v appearing in Equation 21 takes the random vector X_t as its argument, $Y_t := v(X_t, t)$ shall also be understood as a random variable. The dynamics of this random variable Y_t is characterized by the SDE in Equation 19b. One can check that, *e.g.*, the processes (X_t, Y_t) in Theorem 1 can be recovered from Equations 19 and 20 via

$$f := \sigma^2 \nabla \log \Psi, \quad G := \sigma, \quad h := -\frac{1}{2} \|Z_t\|^2 - V, \quad v := \log \Psi.$$

A.2 Main Proofs

Proof of Theorem 1 While Theorem 1 is a direct consequence of the nonlinear Feynman-Kac lemma, here we provide an alternative derivation using standard stochastic calculus. Recall that the optimal SDE on the time coordinate t in Equation 1a, restated below.

$$dX_t = \sigma^2 \nabla \log \Psi(X_t, t) dt + \sigma dW_t, \quad X_0 \sim \mu, \quad X_1 \sim \nu \quad (1a)$$

Apply Itô formula in Equation 18 with $v := \log \Psi(X_t, t)$, where X_t follows Equation 1a,

$$\begin{aligned} d \log \Psi &= \frac{\partial \log \Psi}{\partial t} dt + \left[\nabla \log \Psi \cdot \sigma^2 \nabla \log \Psi + \frac{\sigma^2}{2} \Delta \log \Psi \right] dt + \sigma \nabla \log \Psi \cdot dW_t \\ &= \left[\frac{\partial \log \Psi}{\partial t} + \|\sigma \nabla \log \Psi\|^2 + \frac{\sigma^2}{2} \Delta \log \Psi \right] dt + \sigma \nabla \log \Psi \cdot dW_t, \end{aligned} \quad (22)$$

and notice that the PDE $\frac{\partial \log \Psi}{\partial t}$ obeys

$$\frac{\partial \log \Psi}{\partial t} = \frac{1}{\Psi} \left(-\frac{\sigma^2}{2} \Delta \Psi + V \Psi \right) = -\frac{1}{2} \|\sigma \nabla \log \Psi\|^2 - \frac{\sigma^2}{2} \Delta \log \Psi + V, \quad (23)$$

where the second equality follows from Equation 15. Substituting Equation 23 to Equation 22 yields

$$d \log \Psi = \left[\frac{1}{2} \|\sigma \nabla \log \Psi\|^2 + V \right] dt + \sigma \nabla \log \Psi \cdot dW_t. \quad (24)$$

Now, apply the same Itô formula by instead substituting $v := \log \widehat{\Psi}(X_t, t)$, where X_t again follows Equation 1a,

$$d \log \widehat{\Psi} = \frac{\partial \log \widehat{\Psi}}{\partial t} dt + \left[\nabla \log \widehat{\Psi} \cdot \sigma^2 \nabla \log \Psi + \frac{\sigma^2}{2} \Delta \log \widehat{\Psi} \right] dt + \sigma \nabla \log \widehat{\Psi} \cdot dW_t, \quad (25)$$

and notice that the PDE of $\frac{\partial \log \widehat{\Psi}}{\partial t}$ obeys

$$\frac{\partial \log \widehat{\Psi}}{\partial t} = \frac{1}{\widehat{\Psi}} \left(\frac{\sigma^2}{2} \Delta \widehat{\Psi} - V \widehat{\Psi} \right) = \frac{1}{2} \|\sigma \nabla \log \widehat{\Psi}\|^2 + \frac{\sigma^2}{2} \Delta \log \widehat{\Psi} - V, \quad (26)$$

where the second equality again follows by Equation 15. Substituting Equation 26 to Equation 25 yields

$$\begin{aligned} d \log \widehat{\Psi} &= \left[\frac{1}{2} \|\sigma \nabla \log \widehat{\Psi}\|^2 - V + \sigma^2 \Delta \log \widehat{\Psi} + \sigma^2 \nabla \log \widehat{\Psi} \cdot \nabla \log \Psi \right] dt + \sigma \nabla \log \widehat{\Psi} \cdot dW_t \\ &= \left[\frac{1}{2} \|\sigma \nabla \log \widehat{\Psi}\|^2 - V + \nabla \cdot (\sigma^2 \nabla \log \widehat{\Psi}) + \sigma^2 \nabla \log \widehat{\Psi} \cdot \nabla \log \Psi \right] dt + \sigma \nabla \log \widehat{\Psi} \cdot dW_t. \end{aligned} \quad (27)$$

We conclude the proof by substituting $Y_t := \log \Psi(X_t, t)$ and $\widehat{Y}_t := \log \widehat{\Psi}(X_t, t)$ into Equations 27 and 24. \blacksquare

Proof of Theorem 2 We restrict our focus on $\ell_{\text{fwd}}(\theta, \phi)$, as the derivation of $\ell_{\text{bwd}}(\phi, \theta)$ follows similarly. Let p^θ and p^ϕ denote the path densities induced respectively by the Neural SDEs in Equations 3 and 4, restated below.

$$dX_t^\theta = \sigma Z_t^\theta(X_t^\theta) dt + \sigma dW_t, \quad X_0 \sim \mu \quad (3)$$

$$d\bar{X}_s^\phi = \sigma \widehat{Z}_s^\phi(\bar{X}_s^\phi) ds + \sigma dW_s, \quad \bar{X}_0 \sim \nu \quad (4)$$

We will invoke Girsanov's Theorem (Särkkä and Solin, 2019) to compute the KL divergence between the two path densities, $D_{\text{KL}}(p^\theta || p^\phi)$. Since the theorem necessitates both stochastic processes to be aligned along the *same* time coordinate, we rewrite the stochastic process in Equation 3 with its *reversed* form, following standard practices in, e.g., Anderson (1982)

$$dX_t^\theta = \left[\sigma Z_t^\theta(X_t^\theta) - \sigma^2 \nabla \log p_t^\theta(X_t^\theta) \right] dt + \sigma d\bar{W}_t, \quad X_1^\theta \sim p_1^\theta, \quad (28)$$

where \bar{W}_t is a backward Wiener process along t and p_t^θ denote the marginal density of Equation 3 at time t . Note that Equation 28 is equivalent to Equation 3—in the sense that they yield the same joint distribution and therefore time marginal—except evolving backward in t , or, equivalently, forward in s . With that, the KL divergence can be computed as follows

$$D_{\text{KL}}(p^\theta || p^\phi) = D_{\text{KL}}(p_1^\theta || \nu) + \int_0^1 \mathbb{E}_{p_t^\theta} \left[\frac{1}{2} \|Z_t^\theta - \sigma \nabla \log p_t^\theta + \widehat{Z}_t^\phi\|^2 \right] dt, \quad (29)$$

where the decomposition follows by the chain rule of KL divergence.

Next, we derive the model likelihood $\log \mu^\theta$. Notice that the marginal density $p_t^\theta(x)$ obeys the Fokker Plank equation

$$\frac{\partial p_t^\theta(x)}{\partial t} = -\nabla \cdot \left(p_t^\theta(x) \sigma Z_t^\theta(x) \right) + \frac{\sigma^2}{2} \Delta p_t^\theta(x) \quad (30)$$

$$\begin{aligned} \Rightarrow \frac{\partial \log p_t^\theta}{\partial t} &= \frac{1}{p_t^\theta} \left(-p_t^\theta \nabla \cdot \left(\sigma Z_t^\theta \right) - \nabla p_t^\theta \cdot \sigma Z_t^\theta + \frac{\sigma^2}{2} \Delta p_t^\theta \right) \\ &= -\nabla \cdot \left(\sigma Z_t^\theta \right) - \nabla \log p_t^\theta \cdot \sigma Z_t^\theta + \frac{\sigma^2}{2} \Delta \log p_t^\theta + \frac{1}{2} \|\sigma \nabla \log p_t^\theta\|^2, \end{aligned} \quad (31)$$

where the last equality follows by Equation 15. Now, invoke Itô formula

$$\begin{aligned} d \log p_t^\theta &= \frac{\partial \log p_t^\theta}{\partial t} dt + \left[\nabla \log p_t^\theta \cdot \sigma Z_t^\theta + \frac{\sigma^2}{2} \Delta \log p_t^\theta \right] dt + \sigma \nabla \log p_t^\theta \cdot dW_t \\ &= \left[-\nabla \cdot \left(\sigma Z_t^\theta \right) + \sigma^2 \Delta \log p_t^\theta + \frac{1}{2} \|\sigma \nabla \log p_t^\theta\|^2 \right] dt + \sigma \nabla \log p_t^\theta \cdot dW_t, \end{aligned} \quad (32)$$

where the last equality follows by Equation 31. Equation 32 facilitates a computation of the parametrized model likelihood

$$\begin{aligned} \log \mu^\theta(X_0) &= \mathbb{E}_{p_1^\theta} [\log p_1^\theta(X_1^\theta)] - \int_0^1 \mathbb{E}_{p_t^\theta} [d \log p_t^\theta] \\ &= \mathbb{E}_{p_1^\theta} [\log p_1^\theta(X_1^\theta)] - \int_0^1 \mathbb{E}_{p_t^\theta} \left[-\nabla \cdot \left(\sigma Z_t^\theta \right) + \sigma^2 \Delta \log p_t^\theta + \frac{1}{2} \|\sigma \nabla \log p_t^\theta\|^2 \right] dt \\ &= \mathbb{E}_{p_1^\theta} [\log p_1^\theta(X_1^\theta)] - \int_0^1 \mathbb{E}_{p_t^\theta} \left[-\nabla \cdot \left(\sigma Z_t^\theta \right) - \frac{1}{2} \|\sigma \nabla \log p_t^\theta\|^2 \right] dt, \end{aligned} \quad (33)$$

where the last equality follows by Equation 16. Although Equation 33 implies that the parametrized model likelihood is intractable, due to the unknown score function $\nabla \log p_t^\theta$, combining this likelihood with the KL divergence in Equation 29 yields a tractable objective:

$$\begin{aligned} &D_{\text{KL}}(p^\theta \| p^\phi) - \log \mu^\theta(X_0) \\ &= D_{\text{KL}}(p_1^\theta \| \nu) + \int_0^1 \mathbb{E}_{p_t^\theta} \left[\frac{1}{2} \|Z_t^\theta - \sigma \nabla \log p_t^\theta + \widehat{Z}_t^\phi\|^2 \right] dt \\ &\quad - \mathbb{E}_{p_1^\theta} [\log p_1^\theta(X_1^\theta)] + \int_0^1 \mathbb{E}_{p_t^\theta} \left[-\nabla \cdot \left(\sigma Z_t^\theta \right) - \frac{1}{2} \|\sigma \nabla \log p_t^\theta\|^2 \right] dt \\ &= -\mathbb{E}_{p_1^\theta} [\log \nu(X_1^\theta)] + \int_0^1 \mathbb{E}_{p_t^\theta} \left[\frac{1}{2} \|Z_t^\theta - \sigma \nabla \log p_t^\theta + \widehat{Z}_t^\phi\|^2 - \nabla \cdot \left(\sigma Z_t^\theta \right) - \frac{1}{2} \|\sigma \nabla \log p_t^\theta\|^2 \right] dt \\ &= -\mathbb{E}_{p_1^\theta} [\log \nu(X_1^\theta)] + \int_0^1 \mathbb{E}_{p_t^\theta} \left[\frac{1}{2} \|Z_t^\theta + \widehat{Z}_t^\phi\|^2 - \nabla \cdot \left(\sigma Z_t^\theta \right) - \left(Z_t^\theta + \widehat{Z}_t^\phi \right) \cdot \sigma \nabla \log p_t^\theta \right] dt \\ &= -\mathbb{E}_{p_1^\theta} [\log \nu(X_1^\theta)] + \int_0^1 \mathbb{E}_{p_t^\theta} \left[\frac{1}{2} \|Z_t^\theta + \widehat{Z}_t^\phi\|^2 - \nabla \cdot \left(\sigma Z_t^\theta \right) + \nabla \cdot \left(\sigma Z_t^\theta + \sigma \widehat{Z}_t^\phi \right) \right] dt \\ &= -\mathbb{E}_{p_1^\theta} [\log \nu(X_1^\theta)] + \int_0^1 \mathbb{E}_{p_t^\theta} \left[\frac{1}{2} \|Z_t^\theta + \widehat{Z}_t^\phi\|^2 + \nabla \cdot \left(\sigma \widehat{Z}_t^\phi \right) \right] dt \end{aligned}$$

$$= \ell_{\text{fwd}}(\theta, \phi).$$

Next, we proceed to the minimizer of $\ell_{\text{fwd}}(\theta, \phi)$. Since ϕ appears in $\ell_{\text{fwd}}(\theta, \phi)$ only through the KL divergence in $D_{\text{KL}}(p^\theta || p^\phi)$, ϕ^* must satisfy the following equality (Nelson, 2020)

$$\widehat{Z}_t^{\phi^*} := \sigma \nabla \log p_t^\theta - Z_t^\theta. \quad (34)$$

The remaining objective is thereby

$$\begin{aligned} \ell_{\text{fwd}}(\theta, \phi^*) &= \mathbb{E}_{p_1^\theta}[-\log \nu(X_1^\theta)] + \int_0^1 \mathbb{E}_{p_t^\theta} \left[-\nabla \cdot (\sigma Z_t^\theta) - \frac{1}{2} \|\sigma \nabla \log p_t^\theta\|^2 \right] dt \\ &= \mathbb{E}_{p_1^\theta}[-\log \nu(X_1^\theta)] + \int_0^1 \mathbb{E}_{p_t^\theta} \left[-\nabla \cdot (\sigma Z_t^\theta) + \nabla \cdot \left(\frac{\sigma}{2} Z_t^\theta + \frac{\sigma}{2} \widehat{Z}_t^{\phi^*} \right) \right] dt \\ &= \mathbb{E}_{p_1^\theta}[-\log \nu(X_1^\theta)] - \int_0^1 \mathbb{E}_{p_t^\theta} \left[\nabla \cdot \left(\frac{\sigma}{2} (Z_t^\theta - \widehat{Z}_t^{\phi^*}) \right) \right] dt, \end{aligned} \quad (35)$$

where the second equality follows by Equations 17 and 34. Importantly, Equation 35 is exactly the likelihood objective for a neural ordinary differential equations (ODE) (Grathwohl et al., 2019) with a parameterized vector field $\frac{\sigma}{2}(Z_t^\theta - \widehat{Z}_t^{\phi^*})$. Indeed, the equivalent ODE representation of Equation 3 is known as

$$dX_t^\theta = \frac{\sigma}{2} [Z_t^\theta(X_t^\theta) - \widehat{Z}_t^{\phi^*}(X_t^\theta)] dt,$$

which can be shown by rewriting the Fokker-Plank equation in Equation 30 as

$$\begin{aligned} \frac{\partial p_t^\theta(x)}{\partial t} &= -\nabla \cdot (p_t^\theta(x) \sigma Z_t^\theta(x)) + \frac{\sigma^2}{2} \Delta p_t^\theta(x) \\ &= -\nabla \cdot (p_t^\theta(x) \sigma Z_t^\theta(x) - \frac{\sigma^2}{2} p_t^\theta(x) \nabla \log p_t^\theta(x)) \\ &= -\nabla \cdot (p_t^\theta(x) (\frac{\sigma}{2} Z_t^\theta(X_t^\theta) - \frac{\sigma}{2} \widehat{Z}_t^{\phi^*}(X_t^\theta))), \end{aligned}$$

where the last equality follows by Equation 34. Consequently, the minimizer θ^* achieves

$$\ell_{\text{fwd}}(\theta^*, \phi^*) = -\log \mu, \quad (36)$$

provided the universal approximation theorem of neural networks (Hornik et al., 1989; Csáji et al., 2001). We conclude the proof. \blacksquare

Proof of Theorem 3 Suppose the parametrized functions,

$$Y_t^\theta(x) \equiv Y^\theta(x, t), \quad \widehat{Y}_t^\phi(x) \equiv \widehat{Y}^\phi(x, t), \quad Z_t^\theta(x) := \sigma \nabla Y^\theta(x, t), \quad \widehat{Z}_t^\phi(x) := \sigma \nabla \widehat{Y}^\phi(x, t)$$

satisfy the following set of SDEs

$$dX_t^\theta = \sigma Z_t^\theta(X_t^\theta) dt + \sigma dW_t \quad (37a)$$

$$dY_t^\theta = \left(\frac{1}{2} \|Z_t^\theta(X_t^\theta)\|^2 + V(X_t^\theta, t) \right) dt + Z_t^\theta(X_t^\theta) \cdot dW_t \quad (37b)$$

$$d\widehat{Y}_t^\phi = \left(\frac{1}{2} \|\widehat{Z}_t^\phi(X_t^\theta)\|^2 - V(X_t^\theta, t) + \nabla \cdot (\sigma \widehat{Z}_t^\phi(X_t^\theta)) + Z_t^\theta(X_t^\theta) \cdot \widehat{Z}_t^\phi(X_t^\theta) \right) dt + \widehat{Z}_t^\phi(X_t^\theta) \cdot dW_t \quad (37c)$$

with the boundary conditions

$$X_0 \sim \mu, \quad X_1^\theta \sim p_1^\theta \equiv \nu, \quad Y_0^\theta + \widehat{Y}_0^\phi = \log \mu, \quad Y_1^\theta + \widehat{Y}_1^\phi = \log \nu.$$

Then, it can be readily seen that Equation 37c minimizes $\ell_{\text{TD}}(\phi)$ by construction. On the other hand, Equations 37b and 37c suggest that

$$\begin{aligned} -\left(Y_0^\theta + \widehat{Y}_0^\phi\right) &= -\mathbb{E}_{p_1^\theta} \left[Y_1^\theta + \widehat{Y}_1^\phi \right] + \int_0^1 \mathbb{E}_{p_t^\theta} \left[dY_t^\theta + d\widehat{Y}_t^\phi \right] \\ \Rightarrow -\log \mu(X_0) &= -\mathbb{E}_{p_1^\theta} \left[\log \nu(X_1^\theta) \right] + \int_0^1 \mathbb{E}_{p_t^\theta} \left[\frac{1}{2} \|Z_t^\theta + \widehat{Z}_t^\phi\|^2 + \nabla \cdot (\sigma \widehat{Z}_t^\phi) \right] dt, \end{aligned}$$

implying $\ell_{\text{fwd}}(\theta, \phi)$ is also minimized due to Equation 36. This concludes the necessary condition. For the sufficient condition, we wish to show that $Y_t^{\theta^*}$, $\widehat{Y}_t^{\phi^*}$, $Z_t^{\theta^*}$, and $\widehat{Z}_t^{\phi^*}$ satisfy Equations 37b and 37c given θ^* , ϕ^* that minimize $\ell_{\text{fwd}}(\theta, \phi)$ and $\ell_{\text{TD}}(\phi)$. Since $\ell_{\text{TD}}(\phi^*) = 0$ readily implies Equation 37c, we focus primarily on showing Equation 37b. More precisely, the question pertains to showing that $Y_t^{\theta^*}$ must obey Equation 37b if θ^* solves

$$\begin{aligned} -\log \mu(X_0) &= \min_{\theta} \ell_{\text{fwd}}(\theta, \phi^*) \\ &= \min_{\theta} \left\{ -\mathbb{E}_{p_1^\theta} [\log \nu(X_1^\theta)] + \int_0^1 \mathbb{E}_{p_t^\theta} \left[\frac{1}{2} \|Z_t^\theta + \widehat{Z}_t^{\phi^*}\|^2 + \nabla \cdot (\sigma \widehat{Z}_t^{\phi^*}) \right] dt \right\}. \quad (38) \end{aligned}$$

Now, notice that ϕ^* satisfies

$$\mathbb{E}_{p_1^\theta} [\widehat{Y}_1^{\phi^*}] - \widehat{Y}_0^{\phi^*} = \int_0^1 \mathbb{E}_{p_t^\theta} \left[\frac{1}{2} \|\widehat{Z}_t^{\phi^*}\|^2 - V + \nabla \cdot (\sigma \widehat{Z}_t^{\phi^*}) + Z_t^\theta \cdot \widehat{Z}_t^{\phi^*} \right] dt. \quad (39)$$

Substituting Equation 39 into Equation 38 yields

$$\begin{aligned} -\log \mu(X_0) &= \min_{\theta} \left\{ \mathbb{E}_{p_1^\theta} \left[-\log \nu(X_1^\theta) + \widehat{Y}_1^{\phi^*} \right] - \widehat{Y}_0^{\phi^*} + \int_0^1 \mathbb{E}_{p_t^\theta} \left[\frac{1}{2} \|Z_t^\theta\|^2 + V \right] dt \right\} \\ -\log \mu(X_0) + \widehat{Y}_0^{\phi^*} &= \min_{\theta} \left\{ \mathbb{E}_{p_1^\theta} \left[-\log \nu(X_1^\theta) + \widehat{Y}_1^{\phi^*} \right] + \int_0^1 \mathbb{E}_{p_t^\theta} \left[\frac{1}{2} \|Z_t^\theta\|^2 + V \right] dt \right\}. \quad (40) \end{aligned}$$

Equation 40 is a standard stochastic optimal control problem (Exarchos and Theodorou, 2018; Pereira et al., 2019b), whose optimality condition is known to obey

$$dY_t^{\theta^*} = \left(\frac{1}{2} \|Z_t^{\theta^*}\|^2 + V \right) dt + Z_t^{\theta^*} \cdot dW_t, \quad -Y_1^{\theta^*} = -\log \nu + \widehat{Y}_1^{\phi^*}, \quad -Y_0^{\theta^*} = -\log \mu + \widehat{Y}_0^{\phi^*},$$

which recovers Equation 37b and the boundary conditions. We conclude the proof. \blacksquare

Appendix B. Additional Clarifications

B.1 Optimality conditions of GSBs

Here, we provide a concise derivation of how the PDEs Equation 2 emerges from the variational formulation of GSBs Equation 10 as the *optimality conditions*. We refer readers to, *e.g.*, Chen et al. (2015) and Liu et al. (2022) for a complete treatment. We begin by rewriting the SDE constraint in Equation 10 with the diffusion-transport, *i.e.*, Fokker-Plank, equation

$$\partial_t \rho + \nabla \cdot (\sigma u \rho) - \frac{1}{2} \sigma^2 \Delta \rho, \quad \rho_0 = \mu, \quad \rho_1 = \nu, \quad (41)$$

where $\rho \equiv \rho(x, t)$ is the marginal density at time t , induced by the stochastic controlled process. The Lagrangian formulation of Equation 10 thereby reads

$$\begin{aligned} \mathcal{L}(\rho, u, \lambda) = & \int_{\mathbb{R}^d \times [0,1]} \left[\frac{1}{2} \|u(x, t)\|^2 + V(x, t) \right] \rho(x, t) dx dt \\ & - \int_{\mathbb{R}^d \times [0,1]} \left[\partial_t \rho + \nabla \cdot (\sigma u \rho) - \frac{1}{2} \sigma^2 \Delta \rho \right] \lambda(x, t) dx dt, \end{aligned}$$

where $\lambda(x, t)$ is the Lagrange multiplier and $\rho(x, t)$ are constrained such that $\rho_0 = \mu, \rho_1 = \nu$. Under mild conditions (Anderson, 1982; Yong and Zhou, 1999) such that $\rho(x, t)$ approaches zero at a sufficient speed as $\|x\| \rightarrow \infty$, applying integration by parts yields another PDE that, together with Equation 41, constitutes the optimality conditions to Equation 10

$$\partial_t \lambda - \frac{1}{2} \sigma^2 \|\nabla \lambda\|^2 + \frac{1}{2} \sigma^2 \Delta \lambda + V = 0. \quad (42)$$

The optimal control to Equation 10 is obtained by $u^*(x, t) = -\sigma \nabla \lambda(x, t)$. Notice that Equation 42 is exactly the HJB equation, except its boundary condition is defined *implicitly* through Equation 41, which are constrained by μ and ν at the boundaries. Hence, the PDEs in Equations 41 and 42 can be understood respectively as the conditions to an “optimal” “transport” problem. The PDEs in Equation 2 emerge from Equations 41 and 42 through a change of variables known as the Hopf-Cole transform (Hopf, 1950; Cole, 1951)

$$\Psi(x, t) := \exp(-\lambda(x, t)), \quad \widehat{\Psi}(x, t) := \rho(x, t) \exp(\lambda(x, t)). \quad (43)$$

In other words, the two sets of PDEs in Equations 41 and 42 and Equation 2 are equivalent. The Hopf-Cole transform in Equation 43 also suggests that $\Psi(x, t) \widehat{\Psi}(x, t) = \rho(x, t)$ holds not only at the boundaries but for all $t \in [0, 1]$.

Summarizing, GSBs solve the variational problems in Equation 10, whose optimality conditions are characterized by Equations 41 and 42, or, equivalently, the coupled PDEs in Equation 2. Given $(\Psi, \widehat{\Psi})$ that solve Equation 2, the optimal SDEs can be simulated via Equation 1.

B.2 Implementation Details

While it is theoretically sufficient to parametrize $(Y^\theta, \widehat{Y}^\phi)$ and then infer $Z^\theta := \sigma \nabla Y^\theta$ and $\widehat{Z}^\phi := \sigma \nabla \widehat{Y}^\phi$, we have empirically found that parametrizing $(Z^\theta, \widehat{Z}^\phi)$ with two additional

neural networks often provides extra robustness. This choice introduces additional objectives, namely $\|Z^\theta - \sigma \nabla Y^\theta\|^2$ and $\|\hat{Z}^\phi - \sigma \nabla \hat{Y}^\phi\|^2$, to ensure the alignment of, for instance, $Y^\theta \approx \log \Psi$ and $Z^\theta \approx \sigma \nabla \log \Psi$. In such cases, (Z^θ, \hat{Z}^ϕ) share the same architectures as (Y^θ, \hat{Y}^ϕ) except that the last fully-connected layer outputs vectors in \mathbb{R}^d .

The Neural SDEs are discretized using the Euler-Maruyama method for computing the TD objectives as well as during inference. For generative modeling, we discretize the time interval into 100 steps for MNIST and CelebA, and 200 steps for Cifar10. For crowd navigation MFGs, we consider 100 steps for GMM and 300 steps for V-neck and S-tunnel. Regarding evaluation, the FID scores reported in Figure 3B use 10,000 generated images. Finally, we set the hyper-parameter c appearing in V_{obs} to 3,000 for GMM and 1,500 for the other two MFG problems.

References

- Yves Achdou, Francisco J Buera, Jean-Michel Lasry, Pierre-Louis Lions, and Benjamin Moll. Partial differential equation models in macroeconomics. *Philosophical Transactions of the Royal Society A: Mathematical, Physical and Engineering Sciences*, 372(2028): 20130397, 2014.
- Yves Achdou, Pierre Cardaliaguet, François Delarue, Alessio Porretta, Filippo Santambrogio, Yves Achdou, and Mathieu Laurière. Mean field games and applications: Numerical aspects. *Mean Field Games*, pages 249–307, 2020.
- Yves Achdou, Jiequn Han, Jean-Michel Lasry, Pierre-Louis Lions, and Benjamin Moll. Income and wealth distribution in macroeconomics: A continuous-time approach. *The Review of Economic Studies*, 89(1):45–86, 2022.
- Josh Achiam, Steven Adler, Sandhini Agarwal, Lama Ahmad, Ilge Akkaya, Florencia Leoni Aleman, Diogo Almeida, Janko Altmenschmidt, Sam Altman, Shyamal Anadkat, et al. GPT-4 technical report. *arXiv preprint arXiv:2303.08774*, 2023.
- Brian DO Anderson. Reverse-time diffusion equation models. *Stochastic Processes and their Applications*, 12(3):313–326, 1982.
- Richard Bellman. The theory of dynamic programming. Technical report, Rand corp santa monica ca, 1954.
- Charlotte Bunne, Stefan G Stark, Gabriele Gut, Jacobo Sarabia Del Castillo, Mitch Levesque, Kjong-Van Lehmann, Lucas Pelkmans, Andreas Krause, and Gunnar Rätsch. Learning single-cell perturbation responses using neural optimal transport. *Nature Methods*, 20(11):1759–1768, 2023.
- Kenneth Caluya and Abhishek Halder. Wasserstein Proximal Algorithms for the Schrödinger Bridge Problem: Density Control with Nonlinear Drift. *IEEE Transactions on Automatic Control*, 2021.
- Ricky T. Q. Chen, Yulia Rubanova, Jesse Bettencourt, and David K Duvenaud. Neural ordinary differential equations. In *Advances in Neural Information Processing Systems (NeurIPS)*, 2018.

- Tianrong Chen, Guan-Hong Liu, and Evangelos A Theodorou. Likelihood training of Schrödinger bridge using forward-backward SDEs theory. In *International Conference on Learning Representations (ICLR)*, 2022.
- Yongxin Chen. Density control of interacting agent systems. *IEEE Transactions on Automatic Control*, 2023.
- Yongxin Chen, Tryphon Georgiou, and Michele Pavon. Optimal steering of inertial particles diffusing anisotropically with losses. In *American Control Conference (ACC)*. IEEE, 2015.
- Yongxin Chen, Tryphon T Georgiou, and Michele Pavon. Stochastic Control Liaisons: Richard Sinkhorn Meets Gaspard Monge on a Schrödinger Bridge. *SIAM Review*, 63(2): 249–313, 2021.
- Julian D Cole. On a quasi-linear parabolic equation occurring in aerodynamics. *Quarterly of applied mathematics*, 9(3):225–236, 1951.
- Balázs Csanád Csáji et al. Approximation with artificial neural networks. *Faculty of Sciences, Eötvös Loránd University, Hungary*, 24(48):7, 2001.
- Marco Cuturi. Sinkhorn distances: Lightspeed computation of optimal transport. In *Advances in Neural Information Processing Systems (NeurIPS)*, 2013.
- Marco Cuturi and Arnaud Doucet. Fast computation of Wasserstein barycenters. In *International Conference on Machine Learning (ICML)*, 2014.
- Marco Cuturi, Michal Klein, and Pierre Ablin. Monge, Bregman and Occam: Interpretable optimal transport in high-dimensions with feature-sparse maps. In *International Conference on Machine Learning (ICML)*, 2023.
- Paolo Dai Pra. A stochastic control approach to reciprocal diffusion processes. *Applied Mathematics and Optimization*, 23(1):313–329, 1991.
- Valentin De Bortoli, James Thornton, Jeremy Heng, and Arnaud Doucet. Diffusion Schrödinger bridge with applications to score-based generative modeling. In *Advances in Neural Information Processing Systems (NeurIPS)*, 2021.
- Simone Di Marino, Augusto Gerolin, and Luca Nenna. Optimal transportation theory with repulsive costs. *Topological Optimization and Optimal Transport*, 17:204–256, 2017.
- Ioannis Exarchos and Evangelos A Theodorou. Stochastic optimal control via forward and backward stochastic differential equations and importance sampling. *Automatica*, 87: 159–165, 2018.
- Chris Finlay, Jörn-Henrik Jacobsen, Levon Nurbekyan, and Adam Oberman. How to train your neural ODE: The world of jacobian and kinetic regularization. In *International Conference on Machine Learning (ICML)*, 2020.
- Robert Fortet. Résolution d’un système d’équations de M. Schrödinger. *Journal de Mathématiques Pures et Appliquées*, 19(1-4):83–105, 1940.

- Jason Gaitonde, Jon Kleinberg, and Éva Tardos. Polarization in geometric opinion dynamics. In *ACM Conference on Economics and Computation*, pages 499–519, 2021.
- Will Grathwohl, Ricky T. Q. Chen, Jesse Betterncourt, Ilya Sutskever, and David Duvenaud. FFJORD: Free-form continuous dynamics for scalable reversible generative models. In *International Conference on Learning Representations (ICLR)*, 2019.
- Jiequn Han, Arnulf Jentzen, and E Weinan. Solving high-dimensional partial differential equations using deep learning. *Proceedings of the National Academy of Sciences*, 115(34): 8505–8510, 2018.
- Martin Heusel, Hubert Ramsauer, Thomas Unterthiner, Bernhard Nessler, and Sepp Hochreiter. GANs trained by a two time-scale update rule converge to a local nash equilibrium. In *Advances in Neural Information Processing Systems (NeurIPS)*, 2017.
- Eberhard Hopf. The partial differential equation $u_t + u u_x = \mu x x$. *Communications on Pure and Applied mathematics*, 3(3):201–230, 1950.
- Kurt Hornik, Maxwell Stinchcombe, and Halbert White. Multilayer feedforward networks are universal approximators. *Neural networks*, 2(5):359–366, 1989.
- Kiyosi Itô. *On stochastic differential equations*, volume 4. American Mathematical Soc., 1951.
- Hilbert J Kappen. Path integrals and symmetry breaking for optimal control theory. *Journal of Statistical Mechanics: Theory and Experiment*, 2005(11):P11011, 2005.
- Patrick Kidger, James Foster, Xuechen Li, Harald Oberhauser, and Terry Lyons. Neural sdes as infinite-dimensional GANs. In *International Conference on Machine Learning (ICML)*, 2021.
- Philip A Knight. The Sinkhorn–Knopp algorithm: convergence and applications. *SIAM Journal on Matrix Analysis and Applications*, 30(1):261–275, 2008.
- Magdalena Kobylanski. Backward stochastic differential equations and partial differential equations with quadratic growth. *Annals of probability*, pages 558–602, 2000.
- Soheil Kolouri, Se Rim Park, Matthew Thorpe, Dejan Slepcev, and Gustavo K Rohde. Optimal mass transport: Signal processing and machine-learning applications. *IEEE Signal Processing Magazine*, 34(4):43–59, 2017.
- Takeshi Koshizuka and Issei Sato. Neural Lagrangian Schrödinger bridge: Diffusion modeling for population dynamics. In *International Conference on Learning Representations (ICLR)*, 2023.
- Alex Krizhevsky. Learning multiple layers of features from tiny images. Technical report, 2009.
- Solomon Kullback. Probability densities with given marginals. *The Annals of Mathematical Statistics*, 39(4):1236–1243, 1968.

- Yann LeCun, Corinna Cortes, and CJ Burges. MNIST handwritten digit database. *ATT Labs [Online]*. Available: <http://yann.lecun.com/exdb/mnist>, 2, 2010.
- Christian Léonard. From the Schrödinger problem to the Monge–Kantorovich problem. *Journal of Functional Analysis*, 262(4):1879–1920, 2012.
- Christian Léonard. A survey of the Schrödinger problem and some of its connections with optimal transport. *Discrete and Continuous Dynamical Systems*, 2013.
- Xuechen Li, Ting-Kam Leonard Wong, Ricky T. Q. Chen, and David Duvenaud. Scalable gradients for stochastic differential equations. In *International Conference on Artificial Intelligence and Statistics (AISTATS)*, 2020.
- Alex Tong Lin, Samy Wu Fung, Wuchen Li, Levon Nurbekyan, and Stanley J Osher. Alternating the population and control neural networks to solve high-dimensional stochastic mean-field games. *Proceedings of the National Academy of Sciences*, 118(31), 2021.
- Yaron Lipman, Ricky T. Q. Chen, Heli Ben-Hamu, Maximilian Nickel, and Matt Le. Flow matching for generative modeling. In *International Conference on Learning Representations (ICLR)*, 2023.
- Guan-Hong Liu, Tianrong Chen, Oswin So, and Evangelos A Theodorou. Deep generalized Schrödinger bridge. In *Advances in Neural Information Processing Systems (NeurIPS)*, 2022.
- Zhiyu Liu, Bo Wu, and Hai Lin. A mean field game approach to swarming robots control. In *American Control Conference (ACC)*. IEEE, 2018.
- Ziwei Liu, Ping Luo, Xiaogang Wang, and Xiaoou Tang. Deep learning face attributes in the wild. In *International Conference on Computer Vision (ICCV)*, December 2015.
- Michael Lutter, Shie Mannor, Jan Peters, Dieter Fox, and Animesh Garg. Value iteration in continuous actions, states and time. *arXiv preprint arXiv:2105.04682*, 2021.
- Jin Ma, J-M Morel, and Jiongmin Yong. *Forward-backward stochastic differential equations and their applications*. Number 1702. Springer Science & Business Media, 1999.
- In Jae Myung. Tutorial on maximum likelihood estimation. *Journal of mathematical Psychology*, 47(1):90–100, 2003.
- Edward Nelson. *Dynamical theories of Brownian motion*, volume 106. Princeton university press, 2020.
- Michele Pavon and Anton Wakolbinger. On free energy, stochastic control, and Schrödinger processes. In *Modeling, Estimation and Control of Systems with Uncertainty*, pages 334–348. Springer, 1991.
- Marcus Pereira, Ziyi Wang, Ioannis Exarchos, and Evangelos A Theodorou. Learning deep stochastic optimal control policies using Forward-Backward SDEs. In *Robotics: Science and Systems (RSS)*, 2019a.

- Marcus Pereira, Ziyi Wang, Ioannis Exarchos, and Evangelos A Theodorou. Neural network architectures for stochastic control using the nonlinear feynman-kac lemma. *arXiv preprint arXiv:1902.03986*, 2019b.
- Gabriel Peyré and Marco Cuturi. Computational optimal transport. *Center for Research in Economics and Statistics Working Papers*, 2017.
- Chris Philippidis, Chris Dewdney, and Basil J Hiley. Quantum interference and the quantum potential. *Nuovo Cimento B*, 52(1):15–28, 1979.
- Maziar Raissi, Paris Perdikaris, and George E Karniadakis. Physics-informed neural networks: A deep learning framework for solving forward and inverse problems involving nonlinear partial differential equations. *Journal of Computational physics*, 378:686–707, 2019.
- Lorenz Richter and Julius Berner. Robust SDE-based variational formulations for solving linear PDEs via deep learning. In *International Conference on Machine Learning (ICML)*, 2022.
- Christian P Robert, George Casella, and George Casella. *Monte Carlo statistical methods*, volume 2. Springer, 1999.
- Robin Rombach, Andreas Blattmann, Dominik Lorenz, Patrick Esser, and Björn Ommer. High-resolution image synthesis with latent diffusion models. In *IEEE Conference on Computer Vision and Pattern Recognition (CVPR)*, 2022.
- Lars Ruthotto, Stanley J Osher, Wuchen Li, Levon Nurbekyan, and Samy Wu Fung. A machine learning framework for solving high-dimensional mean field game and mean field control problems. *Proceedings of the National Academy of Sciences*, 117(17):9183–9193, 2020.
- Filippo Santambrogio. Optimal transport for applied mathematicians. *Birkäuser, NY*, 55 (58-63):94, 2015.
- Simo Särkkä and Arno Solin. *Applied stochastic differential equations*, volume 10. Cambridge University Press, 2019.
- Erwin Schrödinger. *Über die Umkehrung der Naturgesetze*, volume IX. Sitzungsberichte der Preuss Akad. Wissen. Phys. Math. Klasse, Sonderausgabe, 1931.
- Erwin Schrödinger. Sur la théorie relativiste de l'électron et l'interprétation de la mécanique quantique. In *Annales de l'institut Henri Poincaré*, volume 2, pages 269–310, 1932.
- Simon Schweighofer, David Garcia, and Frank Schweitzer. An agent-based model of multi-dimensional opinion dynamics and opinion alignment. *Chaos: An Interdisciplinary Journal of Nonlinear Science*, 30(9):093139, 2020.
- Neta Shaul, Ricky T. Q. Chen, Maximilian Nickel, Matthew Le, and Yaron Lipman. On kinetic optimal probability paths for generative models. In *International Conference on Machine Learning (ICML)*, 2023.

- Richard Sinkhorn and Paul Knopp. Concerning nonnegative matrices and doubly stochastic matrices. *Pacific Journal of Mathematics*, 21(2):343–348, 1967.
- Justin Solomon. Optimal transport on discrete domains. *AMS Short Course on Discrete Differential Geometry*, 2018.
- Justin Solomon, Fernando De Goes, Gabriel Peyré, Marco Cuturi, Adrian Butscher, Andy Nguyen, Tao Du, and Leonidas Guibas. Convolutional wasserstein distances: Efficient optimal transportation on geometric domains. *ACM Transactions on Graphics (TOG)*, 34(4):1–11, 2015.
- Yang Song, Jascha Sohl-Dickstein, Diederik P Kingma, Abhishek Kumar, Stefano Ermon, and Ben Poole. Score-based generative modeling through stochastic differential equations. In *International Conference on Learning Representations (ICLR)*, 2021.
- Sanvesh Srivastava, Cheng Li, and David B Dunson. Scalable Bayes via barycenter in Wasserstein space. *Journal of Machine Learning Research (JMLR)*, 19(1):312–346, 2018.
- Csaba Szepesvári. *Algorithms for reinforcement learning*. Springer Nature, 2022.
- Emanuel Todorov. Efficient computation of optimal actions. *Proceedings of the national academy of sciences*, 106(28):11478–11483, 2009.
- Francisco Vargas, Pierre Thodoroff, Neil D Lawrence, and Austen Lamacraft. Solving Schrödinger bridges via maximum likelihood. *Entropy*, 2021.
- Marco A Wiering and Martijn Van Otterlo. Reinforcement learning. *Adaptation, learning, and optimization*, 12(3):729, 2012.
- Jiongmin Yong and Xun Yu Zhou. *Stochastic controls: Hamiltonian systems and HJB equations*, volume 43. Springer Science & Business Media, 1999.